ADVANCED FUNCTIONAL MATERIALS
www.afm-journal.de

Magnetoresistive Memory with Ultralow Critical Current for Magnetization Switching

Nikolay A. Pertsev and Hermann Kohlstedt*

The data writing and thermal stability of information storage are studied theoretically for a magnetic random access memory (MRAM) composed of a magnetic tunnel junction or multilayer exhibiting giant magnetoresistance. The theoretical analysis focuses on the magnetization switching in the "free" layer of a MRAM cell, which is induced by a spin-polarized current imposing a spin-transfer torque (STT) on the magnetization. It is shown that the writing current in such an STT-MRAM reduces dramatically near a spin reorientation transition (SRT) driven by lattice strains and/or surface magnetic anisotropy and even tends to zero under certain conditions. In particular, at the size-driven SRT in the perpendicular-anisotropy CoFeB-MgO tunnel junctions, the critical current densities for magnetization reorientations between the parallel and antiparallel states are expected to fall to low values of about 1.3×10^5 and -3.3×10^4 A cm^{-2}. Remarkably, STT-MRAMs may combine low writing current with very high thermal stability of information storage (retention over 10 years) even at a high density ≈500 Gbit inch^{-2}.

1. Introduction

Magnetic random access memory (MRAM) with non-destructive readout based on the phenomenon of tunneling magnetoresistance (TMR) or giant magnetoresistance (GMR) is a leading contender for the new generation of non-volatile memories.[1,2] An MRAM cell typically comprises two ferromagnetic layers separated by a thin insulating interlayer or nonmagnetic conductive spacer. One of the two layers has a fixed magnetization $\mathbf{M}_{\text{fixed}}$ set to a predetermined direction, whilst the magnetization $\mathbf{M}$ of the other "free" layer can be reoriented by external stimuli for encoding data. The magnetization switching may be accomplished by simply applying an external magnetic field to the free layer, which can be created by an electric current passing past the memory cell. The use of (poorly localized) magnetic fields, however, has serious disadvantages, such as crosstalk between neighboring cells during writing and considerable amount of energy required to switch the magnetization.

Dr. N. A. Pertsev
A. F. Ioffe Physico-Technical Institute
Russian Academy of Sciences
194021 St. Petersburg, Russia
E-mail: pertsev.domain@mail.ioffe.ru
Dr. N. A. Pertsev, Prof. H. Kohlstedt
Nanoelektronik, Technische Fakultät
Christian-Albrechts-Universität zu Kiel
D-24143 Kiel, Germany

DOI: 10.1002/adfm.201200878

Alternatively, the magnetization reorientation can be induced by injecting a spin-polarized current into the free magnetic layer, which imposes a spin-transfer torque (STT) on the magnetization. This method is implemented in the so-called STT-MRAM[1,2] utilizing the STT effect first predicted theoretically[3,4] and then experimentally demonstrated in both GMR multilayers and magnetic tunnel junctions (MTJs).[5–7] Importantly, the current-induced switching eliminates crosstalk between neighboring cells during writing, which makes STT-MRAMs ideally suited for high-density information storage. In addition, the STT-MRAM is fast, has practically unlimited endurance and requires less energy than conventional MRAMs that use magnetic fields for data writing.

Despite these important advantages and several demonstrations of prototype memory cells, industrial applications of STT-MRAMs are still lacking. The main obstacle to commercialization is a high current needed for data writing.[8] Here we show theoretically that the critical current density for the 180° magnetization switching reduces dramatically near a spin-reorientation transition (SRT) between in-plane and perpendicular easy axes. To this end, we analyze the current-induced magnetization dynamics in strained free layers with the account of magnetoelastic coupling and surface magnetic anisotropy. The critical currents destabilizing initial magnetization orientations are calculated for free layers made of ferromagnets with cubic magnetocrystalline anisotropy, which exhibit a strain-driven or size-induced SRT at room temperature. Our calculations also demonstrate that the thermal stability of information storage remains sufficient near the SRT even at a high storage density of about 500 Gbit inch^{-2}. Thus, the major challenge of the present STT-MRAM technology can be solved by the fabrication of memory cells comprising free layers prone to a strain-driven or size-induced SRT.[9]

2. Results and Discussion

2.1. Basic Equations of Magnetization Dynamics

We focus on MTJs and GMR multilayers comprising free and fixed magnetic layers with the typical (001) crystallographic orientation above the Curie temperature (**Figure 1**). Since these layers have nanoscale dimensions, they may be taken

to be homogeneously magnetized up to their saturation magnetizations M_s and M_{fixed}. For the same reason, high lattice strains of up to several percent may be created in magnetic layers by the mechanical interaction with a dissimilar thick substrate.[10–12] Owing to the magnetoelastic coupling,[13,14] these strains **u** may strongly affect the magnetization statics and dynamics in ferromagnetic films.[11,15,16] In the presence of a spin-polarized current with the density J, the magnetization dynamics in a free layer is described by the generalized Landau-Lifshitz-Gilbert equation

$$\frac{d\mathbf{M}}{dt} = -\gamma\mu_0(\mathbf{M}\times\mathbf{H}_{eff}) - \frac{\alpha}{M_s}\left(\mathbf{M}\times\frac{d\mathbf{M}}{dt}\right) + g(\theta)\frac{\mu_B J}{et}\frac{\mathbf{M}\times(\mathbf{M}\times\mathbf{M}_{fixed})}{M_s^2 M_{fixed}}, \quad (1)$$

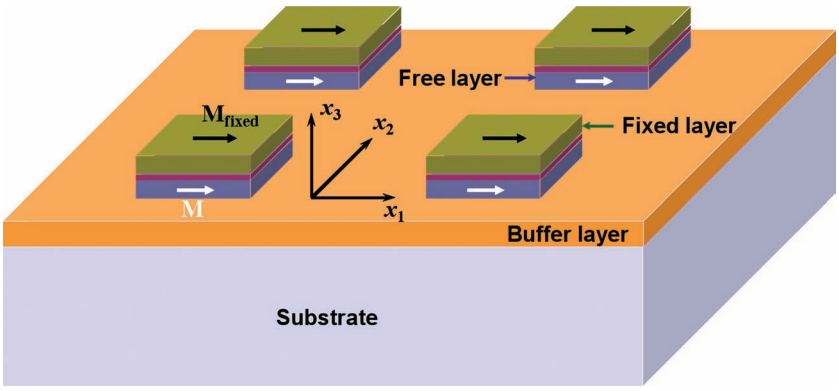

Figure 1. Schematic representation of an array of tunnel junctions with dissimilar ferromagnetic electrodes fabricated on a common substrate. The strain-thickness state of the free magnetic layers is close to the spin reorientation transition between in-plane and out-of-plane magnetization orientations, which provides a drastic reduction of the switching current. A suitable buffer layer may be needed to create lattice strains in free layers ensuring proximity to a strain-driven spin reorientation transition.

where γ is the gyromagnetic ratio, μ_0 is the permeability of the vacuum, e is the electron charge, μ_B is the Bohr magneton, α is the dimensionless damping parameter, and $g(\theta)$ is a scalar function of the included angle θ between the magnetizations **M** and $\mathbf{M}_{fixed}$, which depends on the spin polarization of injected current.[3] The last term in Equation (1) accounts for the spin-transfer torque acting on a free layer with the thickness t. The effective magnetic field $\mathbf{H}_{eff}$ can be calculated from the Helmholtz free energy density F of the free layer as $\mathbf{H}_{eff} = -(1/\mu_0)\partial F/\partial\mathbf{M}$. For cubic ferromagnets considered in this work, the magnetization-dependent part ΔF of the free energy at zero external magnetic fields may be written in the Cartesian reference frame (x_1, x_2, x_3) with the x_3 axis orthogonal to layer surfaces (Figure 1) as

$$\begin{aligned}\Delta F = {} & K_1 m_1^2 m_2^2 + \left(K_1 + \frac{B_1^2}{2c_{11}} - \frac{B_2^2}{2c_{44}}\right)\\ & \times (m_1^2 + m_2^2)m_3^2 + K_2 m_1^2 m_2^2 m_3^2 + \frac{K_s}{t}m_3^2\\ & + B_1(u_{11}m_1^2 + u_{22}m_2^2) + B_2 u_{12} m_1 m_2\\ & - B_1\left[\frac{B_1}{6c_{11}} + \frac{c_{12}}{c_{11}}(u_{11}+u_{22})\right]m_3^2\\ & + \frac{1}{2}\mu_0 M_s^2(N_{11}m_1^2 + N_{22}m_2^2 + N_{33}m_3^2\\ & + 2N_{12}m_1m_2 + 2N_{13}m_1m_3 + 2N_{23}m_2m_3)\\ & - \mu_0 M_s(H_1^{int}m_1 + H_2^{int}m_2 + H_3^{int}m_3),\end{aligned} \quad (2)$$

where m_i (i = 1,2,3) are the direction cosines of **M** with respect to the principal cubic axes x_i ($m_1^2 + m_2^2 + m_3^2 = 1$), N_{ik} form the tensor of demagnetizing factors,[17] K_1 and K_2 are the bulk anisotropy constants of fourth and sixth order at constant strains **u**,[18] K_s is the surface anisotropy constant set equal to the total specific energy of two interfaces, B_1 and B_2 are the magnetoelastic coefficients, and c_{11}, c_{12}, and c_{44} are the elastic stiffnesses at constant magnetization. The last term in Equation (2) allows for the magnetic coupling between the free and fixed layers, which is quantified via the introduction of an effective interaction field $\mathbf{H}_{int}$. When the long-range magnetostatic interaction dominates over the Néel "orange-peel" coupling[19] in an MTJ or the Ruderman–Kittel–Kasuya–Yosida (RKKY) exchange coupling[20] in a GMR multilayer, $\mathbf{H}_{int}$ may be set equal to the mean magnetic field created in the free layer by the fixed one. Differentiating Equation (2), one readily finds the derivatives $\partial\Delta F/\partial m_i$ defining the effective field $\mathbf{H}_{eff}$.

2.2. Strain-Driven and Size-Induced Spin Reorientation Transitions

By calculating the torques created by $\mathbf{H}_{eff}$ and setting them to zero, we can determine the initial magnetization orientation in the free layer. From Equation (2) it follows that this orientation generally varies with the strain state and thickness of the free layer, changing between in-plane ($m_3 = 0$) and perpendicular-to-plane ($m_3 = 1$) directions. In the most important case of an isotropic biaxial strain ($u_{11} = u_{22} = u_m$, $u_{12} = 0$), the reorientation between these directions in a single magnetic layer ($\mathbf{H}_{int} = 0$) occurs abruptly in ferromagnetic materials with $K_1 > 0$ and gradually in ferromagnets with $K_1 < 0$.[18] In MTJs and GMR multilayers, however, the coupling between different magnetic layers may significantly modify such spin reorientation transitions (SRTs). The calculations show that, when the fixed layer in a memory cell has an in-plane magnetization and $|\mathbf{H}_{int}| \ll M_s$, the free layer with $K_1 > 0$ experiences an SRT at a critical strain

$$u_m^*(t) \cong \frac{c_{11}}{B_1(c_{11}+2c_{12})}\left[\frac{1}{2}\mu_0 M_s^2(N_{33}-N_{11}) + \frac{K_s}{t} - \frac{B_1^2}{6c_{11}} \pm \mu_0 M_s\left|H_1^{int}\right|\right], \quad (3)$$

where the magnetostatic shape anisotropy is assumed to favor the [100] magnetization orientation ($N_{11} < N_{22} \ll N_{33}$, $N_{12} = N_{13} = N_{23} = 0$), $\mathbf{M}_{fixed}$ is taken to be parallel to the x_1 axis so

that $H_1^{int} \neq 0$ whilst $H_2^{int} = H_3^{int} = 0$, and the upper and lower signs here and below correspond to the free layer states with orientations of **M** favored and disadvantaged by the coupling with the fixed layer, respectively. In cells with the fixed layer magnetized along the normal to its surfaces ($H_1^{int} = H_2^{int} = 0$, $H_3^{int} \neq 0$), the SRT in the free layer takes place at a slightly different critical strain, which can be calculated from the modified Equation (3), where the last term in square brackets is replaced by $\mp\mu_0 M_s |H_3^{int}|$.

In a single free layer with $K_1 < 0$, the magnetization orientation varies in the strain range limited by the values u_m^* and u_m^{**}, at which **M** becomes parallel and orthogonal to the layer surfaces, respectively.[18] Owing to the coupling with the fixed layer having an in-plane magnetization, the critical strain u_m^* changes to

$$u_m^*(t) = \frac{c_{11}}{B_1(c_{11}+2c_{12})}\left[\frac{1}{2}\mu_0 M_s^2(N_{33}-N_{11}-N_{12}) + \frac{K_1}{2} + \frac{K_2}{4} + \frac{K_s}{t} + \frac{B_1^2}{3c_{11}} - \frac{B_2^2}{2c_{44}} \pm \frac{\sqrt{2}}{2}\mu_0 M_s \left|H_1^{int}\right|\right], \quad (4)$$

where $\mathbf{M}_{fixed}$ is assumed to be parallel to the [110] crystallographic direction in the free layer ($H_1^{int} = H_2^{int} \neq 0$, $H_3^{int} = 0$), which is favored by the shape anisotropy ($N_{11} = N_{22} << N_{33}$, $N_{12} < 0$, $N_{13} = N_{23} = 0$). When the fixed layer has a perpendicular magnetization $\mathbf{M}_{fixed}$ ($H_1^{int} = H_2^{int} = 0$, $H_3^{int} \neq 0$), at the critical strain

$$u_m^{**}(t) = \frac{c_{11}}{B_1(c_{11}+2c_{12})}\left[\frac{1}{2}\mu_0 M_s^2(N_{33}-N_{11}-N_{12}) - K_1 + \frac{K_s}{t} - \frac{2B_1^2}{3c_{11}} + \frac{B_2^2}{2c_{44}} \mp \frac{1}{2}\mu_0 M_s \left|H_3^{int}\right|\right] \quad (5)$$

an in-plane magnetization component with $m_1 = m_2$ appears in the free layer in addition to the perpendicular one.

Besides strain-induced SRTs, a thickness-driven transition may occur in ultrathin magnetic layers.[21] When $K_1 > 0$ and $\mathbf{M}_{fixed}$ is parallel to the x_1 axis, this SRT takes place at a critical thickness

$$t^*(u_m) = 2K_s\left[\mu_0 M_s^2(N_{11}-N_{33}) + \frac{B_1^2}{3c_{11}} + 2B_1\left(1+2\frac{c_{12}}{c_{11}}\right)u_m \mp 2\mu_0 M_s \left|H_1^{int}\right|\right]^{-1} \quad (6)$$

in the following two situations: i) in a magnetic layer with $K_s > 0$ subjected to the misfit strain u_m favoring the out-of-plane magnetization state and ii) in a magnetic layer with $K_s < 0$ having u_m that favors an in-plane magnetization direction. In the case of negative K_1, a size-driven SRT may take place either at the critical thickness t^* defined by the relation

$$t^*(u_m) = 2K_s\left[\mu_0 M_s^2(N_{11}+N_{12}-N_{33}) - K_1 - \frac{K_2}{2} - \frac{2B_1^2}{3c_{11}} + \frac{B_2^2}{c_{44}} + 2B_1\left(1+2\frac{c_{12}}{c_{11}}\right)u_m \mp \sqrt{2}\mu_0 M_s \left|H_1^{int}\right|\right]^{-1} \quad (7)$$

or at the thickness t^{**} given by

$$t^{**}(u_m) = 2K_s\left[\mu_0 M_s^2(N_{11}+N_{12}-N_{33}) + 2K_1 + \frac{4B_1^2}{3c_{11}} - \frac{B_2^2}{c_{44}} + 2B_1\left(1+2\frac{c_{12}}{c_{11}}\right)u_m \pm \mu_0 M_s \left|H_3^{int}\right|\right]^{-1}. \quad (8)$$

Equation (7) corresponds to the SRT at which an out-of-plane magnetization component appears in a memory cell with the fixed layer magnetized along the in-plane [110] direction, whereas Equation (8) defines the thickness at which additional in-plane magnetization with $m_1 = m_2$ arises in the free layer coupled to the fixed layer with a perpendicular magnetization.

2.3. Critical Current Density near Spin Reorientation Transitions

We concentrate now on a typical memory cell, where two stable states correspond to parallel (P) and antiparallel (AP) magnetizations of free and fixed layers, and first consider ferromagnets with positive magnetocrystalline anisotropy. When the strain-thickness conditions in a free layer favor in-plane magnetizations, the vector **M** is parallel to the [100] or [010] crystallographic axis in the usual case of $u_{12} = 0$.[18] Using Equations (1) and (2), we obtain the following system of linearized equations describing the current-induced dynamics of **M** near the initial [100] orientation favored by the shape anisotropy:

$$\frac{dm_2}{dt} = -\frac{\gamma\alpha}{M_s}\left[\mu_0 M_s^2(N_{11}-N_{22}) - 2K_1 + 2B_1(u_{11}-u_{22}) \mp \mu_0 M_s H_1^{int} \mp \frac{\hbar\tilde{g}}{\alpha e t}J\right]m_2 \pm \frac{\gamma}{M_s}\left[\mu_0 M_s^2(N_{11}-N_{33}) - 2K_1 - \frac{2K_s}{t} - \frac{2B_1^2}{3c_{11}} + \frac{B_2^2}{c_{44}} + 2B_1 u_{11} + 2B_1\frac{c_{12}}{c_{11}}(u_{11}+u_{22}) \mp \mu_0 M_s H_1^{int}\right]m_3, \quad (9)$$

$$\frac{dm_3}{dt} = \mp\frac{\gamma}{M_s}\left[\mu_0 M_s^2(N_{11}-N_{22}) - 2K_1 + 2B_1(u_{11}-u_{22}) \mp \mu_0 M_s H_1^{int}\right]m_2 - \frac{\gamma\alpha}{M_s}\left[\mu_0 M_s^2(N_{11}-N_{33}) - 2K_1 - \frac{2K_s}{t} - \frac{2B_1^2}{3c_{11}} + \frac{B_2^2}{c_{44}} + 2B_1 u_{11} + 2B_1\frac{c_{12}}{c_{11}}(u_{11}+u_{22}) \mp \mu_0 M_s H_1^{int} \mp \frac{\hbar\tilde{g}}{\alpha e t}J\right]m_3. \quad (10)$$

Here the upper and lower signs correspond to the P and AP states, respectively, $\mathbf{M}_{\text{fixed}}$ is assumed to have a positive projection on the [100] axis, and $\tilde{g} = g(\theta)/g_e$, where θ equals zero or π and g_e is the electron g-factor. The Jacobian matrix **A** of this system of equations has two eigenvalues which determine stability of the P and AP states (fixed points).[22] These eigenvalues can be calculated from the relation $\lambda_{1,2} = [\text{tr}(\mathbf{A}) \pm \sqrt{\text{tr}(\mathbf{A})^2 - 4\det(\mathbf{A})}]/2$, where tr(**A**) and det(**A**) are the trace and determinant of the Jacobian. Using Equations (9) and (10), it can be shown that the quantity under the square root in this relation does not depend on the current density J. Since a fixed point is stable only when real parts of both eigenvalues are negative,[22] the critical current density J_c destabilizing the P or AP state can be found from the condition tr(**A**) = 0 at tr(**A**)^2–4 det(**A**) < 0 or from the equation $\text{tr}(\mathbf{A}) = -\sqrt{\text{tr}(\mathbf{A})^2 - 4\det(\mathbf{A})}$ if tr(**A**)^2–4 det(**A**) > 0.

The calculation shows that the trace of the Jacobian goes to zero at the current density

$$J_c = \mp \frac{\alpha e t}{\hbar \tilde{g}} \left[\frac{\mu_0 M_s^2}{2}(-2N_{11} + N_{22} + N_{33}) \pm \mu_0 M_s H_1^{\text{int}} + 2K_1 + \frac{K_s}{t} + \frac{B_1^2}{3c_{11}} - \frac{B_2^2}{2c_{44}} - B_1 \frac{c_{12}}{c_{11}}(u_{11} + u_{22}) - B_1(2u_{11} - u_{22}) \right], \quad (11)$$

where the upper and lower signs here and below correspond to the P and AP states, respectively. Equation (11) demonstrates that J_c is a function of the lattice strains u_{11} and u_{22} in the free layer. In the case of isotropic biaxial strain ($u_{11} = u_{22} = u_m$), at the critical strain u_m^* corresponding to the SRT from an in-plane state disadvantaged by the interlayer magnetic coupling to the [001] orientation, the current density J_c becomes equal to

$$J_c^* = \mp \frac{\alpha e t}{\hbar \tilde{g}} \left[\frac{1}{2}\mu_0 M_s^2 (N_{22} - N_{11}) + 2K_1 + \frac{B_1^2}{2c_{11}} - \frac{B_2^2}{2c_{44}} \right] \quad (12)$$

when the initial magnetization in the free layer is directed against $\mathbf{H}_{\text{int}}$. In the opposite case, an additional term $2\mu_0 M_s \left| H_1^{\text{int}} \right|$ appears in the square brackets, which increases J_c^*. Remarkably, the term proportional to $N_{33} >> N_{22} > N_{11}$ vanishes at the SRT in both cases, which indicates that the critical current density may be reduced dramatically with respect to that of an unstrained free layer. At the size-induced SRT, which may take place in an ultrathin free layer at the critical thickness t^* defined by Equation (6), the current density J_c also reduces to a value given by Equation (12).

To evaluate the magnitude of current reduction, we performed numerical calculations for the $Co_{40}Fe_{60}$ alloy, which can be regarded as a model of CoFeB electrodes providing giant TMR ratios in magnetic tunnel junctions.[1] Using the set of material parameters compiled in Ref.[23] ($M_s = 1.8 \times 10^6$ A m^{-1}, $K_1 = 1.3 \times 10^4$ J m^{-3}, $K_2 = 0$, $B_1 = -29.4 \times 10^6$ J m^{-3}, $B_2 = -3 \times 10^6$ J m^{-3}, $c_{11} = 2.8 \times 10^{11}$ N m^{-2}, $c_{12} = 1.4 \times 10^{11}$ N m^{-2}, $c_{44} = 1 \times 10^{11}$ N m^{-2}), we calculated the dependence of J_c on the misfit strain u_m for thick $Co_{40}Fe_{60}$ free layers with $\mathbf{M}_s$ directed against $\mathbf{H}_{\text{int}}$. **Figure 2**a shows that the current density J_c indeed reduces dramatically in the proximity of the strain-induced SRT, decreasing down to ≈1–10% of $J_c^0 = J_c(u_m = 0)$ at $u_m = u_m^*$. It also

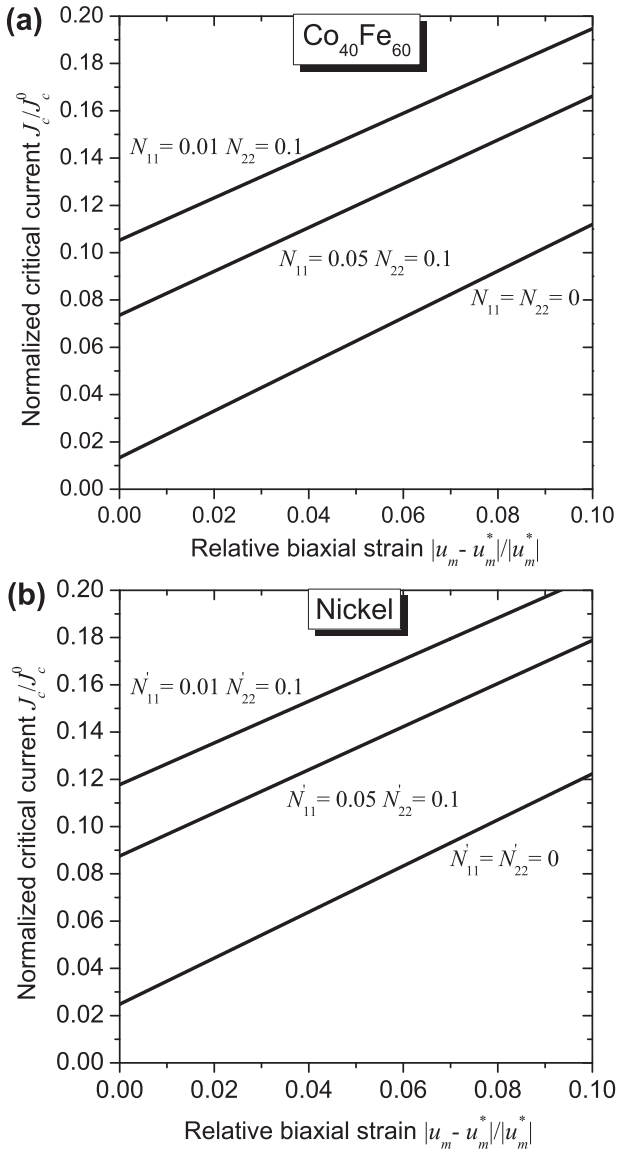

Figure 2. Variation of the normalized critical current $J_c(u_m)/J_c^0$ with the relative biaxial strain $|u_m - u_m^*|/|u_m^*|$ calculated for thick $Co_{40}Fe_{60}$ (a) and Ni (b) free layers with in-plane magnetizations at different values of the in-plane demagnetizing factors indicated on the plots.

demonstrates that the ratio $J_c(u_m^*)/J_c^0$ strongly depends on the shape of the free layer, decreasing when the demagnetizing factors N_{11} and N_{22} become smaller and closer in magnitude. The numerical calculations also confirm that the quantity tr(**A**)^2–4 det(**A**) is negative for $Co_{40}Fe_{60}$ layers with in-plane magnetizations. Therefore, J_c given by Equation (11) represents the sought critical current density destabilizing the P or AP state.

The numerical calculations also show that the interlayer magnetic coupling normally cannot create strong difference between the critical currents needed for the P → AP and AP → P switching processes. Indeed, the experimental data[19] demonstrate that the Néel "orange-peel" coupling gives rise to the interaction field $H_{\text{int}} \leq 50$ Oe ≅ 4×10^3 A m^{-1}so that the

term $2\mu_0 M_s \left|H_1^{\text{int}}\right| \leq 1.8 \times 10^4$ J m^{-3} is one order of magnitude smaller than $\mu_0 M_s^2 (N_{22} - N_{11})/2 \cong 2 \times 10^5$ J m^{-3} at $N_{22} = 0.1 >> N_{11}$. In GMR multilayers, the maximum value of the oscillatory RKKY coupling corresponds to a field with $|H_{\text{int}}| \approx 3.5 \times 10^4$ A m^{-1}, but it may be diminished by choosing appropriate thickness of the nonmagnetic spacer.[20] Finally, the magnetostatic coupling between the free and fixed layers is very small in memory cells with the in-plane size $L_1 > 1$ μm but has a tendency to increase rapidly with decreasing L_1.[24] Extrapolating the experimental data reported in Ref.[24], we can estimate the magnetostatic interaction field to be $\approx 1.5 \times 10^4$ A m^{-1} at $L_1 = 100$ nm and $\approx 3 \times 10^4$ A m^{-1} at $L_1 = 40$ nm. Thus, owing to the interlayer magnetic coupling, the switching currents for the P → AP and AP → P reorientations may differ by a factor of order 2.

In the case of ferromagnetic layers magnetized in the direction orthogonal to their surfaces, the current-induced dynamics of **M** near the initial [001] orientation is described by a system of equations similar to Equations (9) and (10). For the critical current density, the calculation gives

$$J_c = \mp \frac{\alpha e t}{\hbar \tilde{g}} \left[\frac{\mu_0 M_s^2}{2} (N_{11} + N_{22} - 2N_{33}) \pm \mu_0 M_s H_3^{\text{int}} + 2K_1 - \frac{2K_s}{t} + \frac{4B_1^2}{3c_{11}} - \frac{B_2^2}{c_{44}} + \frac{B_1}{c_{11}} (c_{11} + 2c_{12})(u_{11} + u_{22}) \right]. \quad (13)$$

It can be seen that, in the memory cell with "perpendicular" easy axis, the magnetostatic term proportional to $N_{33} >> N_{22} > N_{11}$ reduces the critical current, while the interface anisotropy $K_s < 0$ stabilizing the out-of-plane orientation of **M** should increase J_c. At the isotropic biaxial strain u_m^* corresponding to the abrupt SRT from the [001] to [100] magnetization orientation ($N_{11} \leq N_{22}$), the current density J_c becomes

$$J_c^* = \mp \frac{\alpha e t}{\hbar \tilde{g}} \left[\frac{1}{2} \mu_0 M_s^2 (N_{22} - N_{11}) + 2K_1 + \frac{B_1^2}{c_{11}} - \frac{B_2^2}{c_{44}} + n\mu_0 M_s \left|H_3^{\text{int}}\right| \right], \quad (14)$$

where $n = 1$ for the P → AP or AP → P switching facilitated by the interlayer magnetic coupling and $n = 3$ in the opposite case. Equation (14) shows that the current density J_c^* is independent of both N_{33} and K_s. At the size-induced SRT, J_c also reduces to values given by Equation (14).

Using Equation (13) and the experimental data reported by Ikeda et al.,[25] we can estimate the absolute values of J_c^* for the $Co_{20}Fe_{60}B_{20}/MgO/Co_{20}Fe_{60}B_{20}$ tunnel junctions. Here a size-induced SRT between in-plane and perpendicular magnetization orientations takes place in a single $Co_{20}Fe_{60}B_{20}$ layer at the thickness $t^* \approx 1.5$ nm due to strong interfacial anisotropy with $K_s \approx -1.3$ mJ m^{-2}. This critical thickness can be reproduced with a good accuracy by Equation (6) if we set $H_1^{\text{int}} = 0$, $u_{11} = u_{22} = 0$, and substitute the measured saturation magnetization $M_s \approx 1.26 \times 10^6$ A m^{-1} of $Co_{20}Fe_{60}B_{20}$ and the calculated demagnetizing factors $N_{11} = N_{22} = 0.05$. The interlayer magnetic coupling in the tunnel junction can be estimated from the data shown in Figure 5a of ref. [25], which gives $\left|H_3^{\text{int}}\right| \approx 4 \times 10^3$ A m^{-1}, and the anisotropy constant K_1 of $Co_{20}Fe_{60}B_{20}$ may be approximated by that of $Co_{40}Fe_{60}$. Then the thickness dependence of the critical current density J_c can be found from Equation (13), where the measured values $\alpha(t)$ should be used for the damping constant.[25] The calculation shows that, when the free layer thickness increases from $t = 1$ nm to the critical thickness t^*, J_c reduces by a factor of 45 for the P → AP switching and by a factor of 60 for the AP→P one. Since for these two magnetization reorientations $J_c = 5.8 \times 10^6$ and -2×10^6 A cm^{-2} at $t = 1$ nm,[25] we find that the critical current densities are expected to fall down to low values of $J_c^*(\text{P} \rightarrow \text{AP}) \approx 1.3 \times 10^5$ A cm^{-2} and $J_c^*(\text{AP} \rightarrow \text{P}) \approx -3.3 \times 10^4$ A cm^{-2} at the size-driven SRT in these junctions.

The strain/size-induced reduction of the critical current also takes place in ferromagnets with negative magnetocrystalline anisotropy ($K_1 < 0$). To demonstrate this effect, let us consider the most important case of a free layer subjected to an isotropic biaxial strain ($u_{11} = u_{22} = u_m$, $u_{12} = 0$). At the strain-thickness conditions ensuring an in-plane magnetization orientation, **M** tends to be parallel to one of in-plane face diagonals of the unit cell.[18] Therefore, we take the magnetizations **M** and $\mathbf{M}_{\text{fixed}}$ of two magnetic layers to be initially parallel to the [110] crystallographic axis of the free layer, assuming that this orientation is favored by the magnetostatic shape anisotropy ($N_{11} = N_{22}$, $N_{12} < 0$). The system of equations describing the current-induced magnetization dynamics near the [110] direction simplifies in the rotated reference frame with the x_1' axis parallel to the [110] axis, where it becomes similar to Equations (9) and (10). The calculation shows that the trace of the Jacobian matrix of this system of equations goes to zero at the current density

$$J_c = \mp \frac{\alpha e t}{\hbar \tilde{g}} \left[\frac{1}{2} \mu_0 M_s^2 (-2N_{11}' + N_{22}' + N_{33}) \pm \sqrt{2} \mu_0 M_s H_1^{\text{int}} - \frac{K_1}{2} + \frac{K_2}{4} + \frac{K_s}{t} + \frac{B_1^2}{3c_{11}} - \frac{B_2^2}{2c_{44}} - B_1 \left(1 + 2\frac{c_{12}}{c_{11}}\right) u_m \right], \quad (15)$$

where $N_{11}' = N_{11} + N_{12}$ and $N_{22}' = N_{11} - N_{12}$ denote the demagnetizing factors of the free layer in the rotated reference frame (x_1', x_2', x_3). At the critical strain u_m^* given by Equation (4) and the critical thickness t^* defined by Equation (7), the current density J_c reduces to $J_c^* = \mp(\alpha e t/\hbar \tilde{g})[\mu_0 M_s^2 (N_{22}' - N_{11}')/2 + n\mu_0 M_s \left|H_1^{\text{int}}\right|/\sqrt{2} - K_1]$, where $n = -1$ for the P → AP or AP → P switching facilitated by the interlayer magnetic coupling and $n = 3$ in the opposite case.

We have chosen Ni as a representative material with negative magnetocrystalline anisotropy because NiFe and NiFeB electrodes are employed in MTJs as well.[1,24,26] Using the set of material parameters collected in ref. [18] ($M_s = 4.85 \times 10^5$ A m^{-1}, $K_1 = -0.37 \times 10^4$ J m^{-3}, $K_2 = -0.23 \times 10^4$ J m^{-3}, $B_1 = 9.2 \times 10^6$ J m^{-3}, $B_2 = 10.2 \times 10^6$ J m^{-3}, $c_{11} = 2.465 \times 10^{11}$ N m^{-2}, $c_{12} = 1.473 \times 10^{11}$ N m^{-2}, $c_{44} = 1.247 \times 10^{11}$ N m^{-2}), we calculated the strain dependence of J_c for thick Ni layers at $\left|H_1^{\text{int}}\right| << |K_1|/(\mu_0 M_s)$. Figure 2b shows that the current density given by Equation (15) also reduces drastically in the proximity of the strain-induced SRT, decreasing down to 2.5 – 12% of J_c^0 at $u_m = u_m^*$. The numerical calculations confirm

that the quantity $\mathrm{tr}(\mathbf{A})^2$–4 $\det(\mathbf{A})$ is negative for Ni layers in the relevant strain range. Taking theoretical values of $\tilde{g}$ predicted by the model of Slonczewski[3] and assuming $\alpha \sim 0.01$,[27] we find that, in Ni junctions similar to MTJs studied in ref. [24] (t = 1.7 nm, $L_1 = L_2 = 2$ μm, $|H_1^{\mathrm{int}}| \approx 10^3$ A m^{-1}), the current density $|J_c^*|$ should be below 2.2×10^5 and 1.2×10^5 A cm^{-2} for the P → AP and AP → P magnetization reorientations, respectively.

The most remarkable phenomenon arises when the free layer made of a ferromagnet with $K_1 < 0$ has the perpendicular magnetization. In this case, the relevant SRT takes place at the critical strain u_m^{**} given by Equation (5) or at the critical thickness t^{**} defined by Equation (8). The substitution of u_m^{**}or t^{**} into Equation (13) shows that the current density needed for the magnetization switching facilitated by the interlayer magnetic coupling becomes equal to $J_c^* = \mp(\alpha et/2\hbar\tilde{g})\mu_0 M_s^2(N'_{22} - N'_{11})$ at the SRT. Hence in circular magnetic layers ($N'_{11} = N'_{22}$) this critical current goes to zero in our approximation, which can be attributed to the fact that the magnetocrystalline anisotropy destabilizes the perpendicular magnetization orientation at $K_1 < 0$. In the vicinity of the discussed second-order transition, the critical current remains much smaller than J_c^0, being below 0.01 J_c^0 at $(u_m - u_m^{**})/u_m^{**} < 0.5\%$ in circular Ni layers.

At the same time, the current density J_c^* corresponding to the magnetization switching hindered by the interlayer magnetic coupling is described by the relation $J_c^* = \mp(\alpha et/2\hbar\tilde{g})\mu_0 M_s\left[M_s(N'_{22} - N'_{11}) + 4\left|H_3^{\mathrm{int}}\right|\right]$ so that it remains finite even in circular layers. The interaction field $\left|H_3^{\mathrm{int}}\right|$ in circular Ni junctions with the diameter ~50 nm is estimated to be $\left|H_3^{\mathrm{int}}\right| \approx 1.5 \times 10^3$ A m^{-1} based on the magnetostatic coupling observed in the $Co_{20}Fe_{60}B_{20}$ junctions[25] corrected by the ratio of Ni and $Co_{20}Fe_{60}B_{20}$ magnetizations. Hence we find that, at the relevant thicknesses $t = 1 - 3$ nm, J_c^* is expected to have low values ranging from 7×10^4 to 2×10^5 A cm^{-2}.

Concluding the discussion of current-induced magnetization switching, we note that the qualitative predictions of our theory should be valid for memory cells with polycrystalline and amorphous free layers as well. These layers differ from single-crystalline ones by much smaller or negligible bulk magnetocrystalline anisotropy, but their magnetoelastic coefficients are comparable to those of corresponding single crystals, being only a few times smaller in some polycrystalline CoFe and amorphous CoFeB alloys.[28] Hence the strain-induced SRTs should occur in polycrystalline and amorphous free layers as well, and the corresponding critical strains can be evaluated using Equation (2) and setting $B_1 = B_2 = B$, $c_{44} = (c_{11} - c_{22})/2$, $K_1 = 2B^2(c_{11} + c_{12})/[(c_{11} - c_{12})(c_{11} + 2c_{12})] > 0$, and $K_2 = 0$, since the average magnetostrictive and elastic properties of untextured layers are isotropic and their magnetocrystalline anisotropy constants $K_{i\sigma}$ at constant stresses may be neglected. Similarly, the surface (interface) magnetic anisotropy was found to be substantial even in amorphous ferromagnetic layers,[29] which indicates that the size-induced SRT may also take place here. Furthermore, all terms in Equation (1) describing the current-induced magnetization dynamics retain their form in the case of polycrystalline and amorphous free layers. Therefore, the critical current density can be evaluated for such layers from Equations (11) and (13) so that it should reduce drastically at the SRT for the same reasons as in single-crystalline layers, being given by Equations (12) and (14) for polycrystalline and amorphous layers with in-plane and perpendicular-to-plane average magnetizations, respectively.

2.4. Thermal Stability of Data Storage

It should be emphasized that the thermal stability of information storage deteriorates in the vicinity of SRT because the magnetization reorientation in the plane orthogonal to layer surfaces becomes easier here. However, the calculation shows that this reorientation is hindered by a potential barrier even at the critical strain ($u_m = u_m^*$) or thickness ($t = t^*$). In ferromagnets with $K_1 > 0$, this barrier separates the energy minima corresponding to in-plane and perpendicular magnetization orientations, and its height U_b^* at $\mathbf{H}_{\mathrm{int}} = 0$ is given by the relation $U_b^* = [K_1/4 + B_1^2/(8c_{11}) - B_2^2/(8c_{44})]V$, where V is the volume of the free layer. In contrast, the potential barrier at $K_1 < 0$ is formed by an energy maximum associated with the perpendicular or in-plane magnetization orientation so that the barrier height equals $U_b^* = [-3K_1/4 - K_2/4 - B_1^2/(2c_{11}) + B_2^2/(2c_{44})]V$ at the critical strain $u_m = u_m^*$ and $U_b^* = [-3K_1/4 - B_1^2/(2c_{11}) + B_2^2/(2c_{44})]V$ at $u_m = u_m^{**}$. For the $Co_{40}Fe_{60}$ and in-plane magnetized Ni layers, the numerical calculations give $U_b^*/V \approx 3600$ J m^{-3}, whilst the Ni layer with perpendicular magnetization has $U_b^*/V \approx 3000$ J m^{-3}. To ensure the thermal stability of magnetization orientation at room temperature T_r, the barrier height must be not less than about 50 $k_B T_r$, where k_B is the Boltzmann constant. Hence the minimum volume of the $Co_{40}Fe_{60}$ or in-plane magnetized Ni layer is about 6×10^4 nm^3, which converts into the layer area $A \sim 2 \times 10^4$ nm^2 at the typical thickness $t = 3$ nm.

Remarkably, the volume of a $Co_{40}Fe_{60}$ layer ensuring thermal stability of information storage reduces rapidly with increasing difference $|u_m - u_m^*|$, because the barrier height $U_b(u_m)$ rises sharply when u_m deviates from u_m^*. As a result, reliable high-density storage becomes possible even at near-critical strains providing drastic reduction of the current density J_c. For example, the stable data storage with a density of about 500 Gbit inch^{-2} ($A \approx 1000$ nm^2) is achieved at $|u_m - u_m^*|/|u_m^*| \approx 2.5\%$ if the demagnetizing factors N_{11} and N_{22} are negligible and at $|u_m - u_m^*|/|u_m^*| \approx 3\%$ when $N_{11} = 0.01 - 0.05$ and $N_{22} = 0.1$. It should be noted that at these strains the potential barrier corresponds either to the perpendicular magnetization orientation ($u_m > u_m^*$) or to the in-plane one ($u_m < u_m^*$) so that the barrier height becomes equal to $U_b = |(\mu_0 M_s^2/2)(N_{33} - N_{11}) + K_s/t - B_1^2/(6c_{11}) - B_1(1 + 2c_{12}/c_{11})u_m|V$.

In practice, the proximity to the strain-induced SRT can be tuned with the aid of a ferroelectric crystal used as a substrate for the fabrication of MTJs or GMR multilayers[30,31] or by attaching a piezoelectric actuator to a conventional substrate (see **Figure 3**). Indeed, the application of an electric field $\mathbf{E}$ to a substrate or actuator with piezoelectric coefficients d_{kij} produces macroscopic deformations $u_{ij}^s = d_{kij}E_k$ here. These deformations induce additional in-plane strains $\delta u_{\alpha\beta}$ ($\alpha,\beta = 1,2$) in the free layer, which add to the lattice strains $u_{\alpha\beta}^0$ created during the fabrication procedure. Remarkably, single crystals of relaxor ferroelectrics, such as $Pb(Zn_{1/3}Nb_{2/3})O_3$–$PbTiO_3$ (PZN-PT) or $Pb(Mg_{1/3}Nb_{2/3})O_3$–$PbTiO_3$ (PMN-PT) having ultrahigh piezoelectric coefficients ~1000 pm V^{-1},[32] can create strains $\delta u_{\alpha\alpha}$ up to 1% in the case of perfect strain transmission across

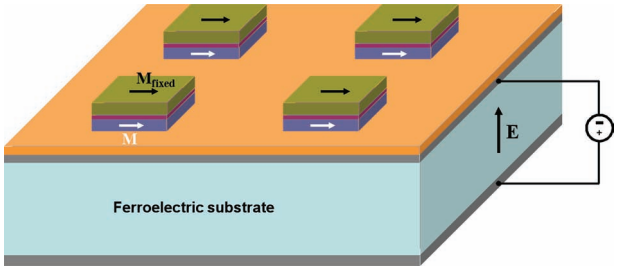

Figure 3. Array of magnetic tunnel junctions fabricated on a common ferroelectric substrate. The application of an electric field to the electrodes deposited on two substrate faces allows fine tuning of lattice strains in free layers of tunnel junctions.

interfaces in the heterostructure.[18] As a result, a wide-range electrical tuning of total in-plane strains $u_{\alpha\alpha} = u^0_{\alpha\alpha} + \delta u_{\alpha\alpha}(\mathbf{E})$ in free layers becomes possible under favorable conditions.

By applying appropriate voltage to a ferroelectric substrate, the switching current may be reduced during the data writing due to enhanced proximity to a strain-driven SRT. Since this voltage can be removed after completion of the writing procedure, free layers of memory cells can be kept in a strain state remote from the SRT while no writing is performed. Hence the electrical tuning of lattice strains makes it possible to increase the thermal stability of information storage as well.

2.5. Effect of Anisotropic Substrate-Induced Strains

Equation (11) suggests that the critical current density for the in-plane magnetized free layer may be further reduced by creating anisotropic in-plane strains $u_{11} \neq u_{22}$ here. These strains can be induced electrically in MTJs and GMR multilayers fabricated on a ferroelectric substrate[30,31] and must promote the in-plane 90° rotation of the free layer magnetization. To this end, the electric field should be applied to the substrate in an appropriate direction, normally taken to be parallel to the substrate face on which magnetic layers are fabricated.[18] In the case of (011)-cut PZN-PT and PMN-PT single crystals poled along their [011] crystallographic direction, however, even an electric field **E** orthogonal to this face creates anisotropic piezoelectric strains $u^s_{11}(\mathbf{E}) \neq u^s_{22}(\mathbf{E})$.[33] Accordingly, the in-plane lattice strains in the free layer with the [100] crystallographic axis parallel to the [100] axis of the substrate become $u_{11}(E_3) = u_m + d_{311}E_3$ and $u_{22}(E_3) = u_m + d_{322}E_3$, where u_m is the isotropic biaxial strain created in the free layer during the fabrication procedure, and perfect strain transmission across interfaces is assumed. **Figure 4** shows the normalized critical current $J_c(E_3)/J_c(E_3 = 0)$ of a thick $Co_{40}Fe_{60}$ layer fabricated on the (011)-cut PZN-6%PT single crystal as a function of electric field intensity E_3 at different values of the initial strain u_m. It can be seen that additional anisotropic strains affect the critical current dramatically at $u_m = u^*_m$, reducing J_c by more than ten times at the maximum field intensity $E_{max} \cong K_1/[B_1(d_{311} - d_{322})] \approx 1$ kV/cm leaving the initial [100] orientation of the magnetization unaltered.[30,31] Importantly, an ultralow voltage of only 0.1 V is needed to create the electric field of 1 kV/cm in a micron-thick PZN-6%PT substrate. However, the effect of anisotropic strains

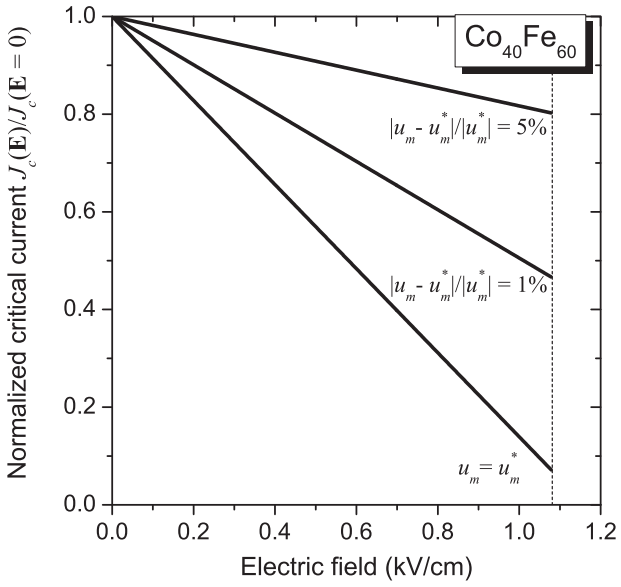

Figure 4. Variation of the normalized critical current $J_c(\mathbf{E})/J_c(\mathbf{E} = 0)$ of a thick $Co_{40}Fe_{60}$ layer with the electric field **E** applied to the (011)-cut PZN-6%PT substrate. Values of the initial isotropic biaxial strain u_m in the $Co_{40}Fe_{60}$ layer are indicated on the plots. The in-plane demagnetizing factors and $\mathbf{H}_{int}$ are assumed to be negligible ($N_{11} = N_{22} = 0$). The piezoelectric coefficients of PZN-6%PT crystal are taken to be $d_{311} = -3000$ pm/V and $d_{322} = 1100$ pm/V.[33] The dashed line shows the maximum electric field $E_{max} \approx 1.08$ kV/cm, which can be applied to the substrate without making the [100] magnetization orientation unstable.

rapidly diminishes with increasing deviation of the initial strain state from the SRT, decreasing down to only 20% already at $|u_m - u^*_m|/|u^*_m| = 5\%$.

Finally, it should be emphasized that the predicted drastic reduction of J_c makes it possible to keep the magnetization switching time τ_{sw} within subnanosecond range at current densities J ensuring ultralow write energy $U_{sw} \sim J^2\tau_{sw}$ on the order of 1fJ per bit. Indeed, even conventional magnetic free layers may display an ultrafast current-induced magnetization reversal with $\tau_{sw} < 1$ ns and moderate power dissipation ($U_{sw} \sim$ 1 pJ).[34] This remarkable feature, however, is achieved only at current densities several times higher than the critical density J_c because the switching time scales as $\tau_{sw} \sim (J-J_c)^{-1}$.[27,35] Hence the reduction of J_c is critical for the development of ultrafast STT-MRAMs with ultralow power consumption.

3. Conclusions

In this work, we demonstrated theoretically that the density of a spin-polarized current needed for the 180° magnetization switching in a free magnetic layer of an MTJ or GMR multilayer reduces drastically in the vicinity of a strain-driven or size-induced SRT. The practical realization of a magnetoresistive memory with low switching current requires the use of free layers having an SRT occurring at experimentally accessible lattice strains or nanoscale layer thickness. Our calculations showed that free layers made of cubic ferromagnets with weak

magnetocrystalline anisotropy and strong magnetoelastic coupling, such as the $Co_{40}Fe_{60}$ alloy, may display reduction of the critical current up to three orders of magnitude. Importantly, a high thermal stability factor $U_b^*/(k_B T_r) \approx 50$ corresponding to retention over ten years on a bit level can be preserved for high-density data storage even under conditions ensuring drastic reduction of the switching current.

Acknowledgements

This work was supported by the Deutsche Forschungsgemeinschaft via the DFG grant INST 257/343-1/570236 (Mercator Visiting Professorship awarded to N.A.P.) and the SFB 855 01/10 entitled "Magnetoelectric Composites – Future Biomagnetic Interfaces".

Received: March 28, 2012
Revised: May 28, 2012
Published online: July 5, 2012

[1] S. Ikeda, J. Hayakawa, Y. M. Lee, F. Matsukura, Y. Ohno, T. Hanyu, H. Ohno, *IEEE Trans. Electron Devices* **2007**, *54*, 991.
[2] Y. M. Huai, *AAPPS Bull.* **2008**, *18*, 33.
[3] J. C. Slonczewski, *J. Magn. Magn. Mater.* **1996**, *159*, L1.
[4] L. Berger, *Phys. Rev. B* **1996**, *54*, 9353.
[5] M. Tsoi, A. G. M. Jansen, J. Bass, W.-C. Chiang, M. Seck, V. Tsoi, P. Wyder, *Phys. Rev. Lett.* **1998**, *80*, 4281.
[6] E. B. Myers, D. C. Ralph, J. A. Katine, R. N. Louie, R. A. Buhrman, *Science* **1999**, *285*, 867.
[7] Y. Huai, F. Albert, P. Nguyen, M. Pakala, T. Valet, *Appl. Phys. Lett.* **2004**, *84*, 3118.
[8] D. C. Ralph, Y.-T. Cui, L. Q. Liu, T. Moriyama, C. Wang, R. A. Buhrman, *Phil. Trans. R. Soc. A* **2011**, *369*, 3617.
[9] N. A. Pertsev, H. Kohlstedt, *Patent application* PCT/EP2011/004016, **2011**.
[10] B. N. Engel, C. D. England, R. A. Van Leeuwen, M. H. Wiedmann, C. M. Falco, *J. Appl. Phys.* **1991**, *70*, 5873.
[11] B. Schulz, K. Baberschke, *Phys. Rev. B* **1994**, *50*, 13467.
[12] H. Lee, I.-G. Baek, E. Vescovo, *Appl. Phys. Lett.* **2006**, *89*, 112516.
[13] N. Akulov, *Z. Phys.* **1928**, *52*, 389.
[14] C. Kittel, *Rev. Mod. Phys.* **1949**, *21*, 541.
[15] M.-T. Lin, J. Shen, W. Kuch, H. Jenniches, M. Klaua, C. M. Schneider, J. Kirschner, *Phys. Rev. B* **1997**, *55*, 5886.
[16] A. Lisfi, C. M. Williams, L. T. Nguyen, J. C. Lodder, A. Coleman, H. Corcoran, A. Johnson, P. Chang, A. Kumar, W. Morgan, *Phys. Rev. B* **2007**, *76*, 054405.
[17] L. D. Landau, E. M. Lifshitz, L. P. Pitaevskii, *Electrodynamics of Continuous Media*, Pergamon, Oxford **1984**.
[18] N. A. Pertsev, *Phys. Rev. B* **2008**, *78*, 212102.
[19] B. D. Schrag, A. Anguelouch, S. Ingvarsson, G. Xiao, Y. Lu, P. L. Trouilloud, A. Gupta, R. A. Wanner, W. J. Gallagher, P. M. Rice, S. S. P. Parkin, *Appl. Phys. Lett.* **2000**, *77*, 2373.
[20] P. Bruno, C. Chappert, *Phys. Rev. Lett.* **1991**, *67*, 1602.
[21] P. J. Jensen, K. H. Bennemann, *Surf. Sci. Rep.* **2006**, *61*, 129.
[22] M. Gmitra, J. Barnaś, *Phys. Rev. Lett.* **2006**, *96*, 207205.
[23] N. A. Pertsev, H. Kohlstedt, R. Knöchel, *Phys. Rev. B* **2011**, *84*, 014423.
[24] K.-S. Moon, R. E. Fontana Jr., S. S. P. Parkin, *Appl. Phys. Lett.* **1999**, *74*, 3690.
[25] S. Ikeda, K. Miura, H. Yamamoto, K. Mizunuma, H. D. Gan, M. Endo, S. Kanai, J. Hayakawa, F. Matsukura, H. Ohno, *Nat. Mater.* **2010**, *9*, 721–724.
[26] J. C. Read, J. J. Cha, W. F. Egelhoff Jr., H. W. Tseng, P. Y. Huang, Y. Li, D. A. Muller, R. A. Buhrman, *Appl. Phys. Lett.* **2009**, *94*, 112504.
[27] D. Bedau, H. Liu, J.-J. Bouzaglou, A. D. Kent, J. Z. Sun, J. A. Katine, E. E. Fullerton, S. Mangin, *Appl. Phys. Lett.* **2010**, *96*, 022514.
[28] J. M. Barandiarán, J. Gutiérrez, A. García-Arribas, *Phys. Status Solidi A* **2011**, *208*, 2258.
[29] R. J. Hicken, G. T. Rado, G. Xiao, C. L. Chien, *Phys. Rev. Lett.* **1990**, *64*, 1820.
[30] N. A. Pertsev, H. Kohlstedt, *Appl. Phys. Lett.* **2009**, *95*, 163503.
[31] N. A. Pertsev, H. Kohlstedt, *Nanotechnology* **2010**, *21*, 475202.
[32] S.-E. Park, T. R. Shrout, *J. Appl. Phys.* **1997**, *82*, 1804.
[33] J. Lou, M. Liu, D. Reed, Y. Ren, N. X. Sun, *Adv. Mater.* **2009**, *21*, 4711.
[34] A. A. Tulapurkar, T. Devolder, K. Yagami, P. Crozat, C. Chappert, A. Fukushima, Y. Suzuki, *Appl. Phys. Lett.* **2004**, *85*, 5358.
[35] J. Z. Sun, *Phys. Rev. B* **2000**, *62*, 570.